4

Pattern Formation in Cancer

J.A. Sherratt[1], **A.J. Perumpanani**[2], **M.R. Owen**[3]

[1] *Department of Mathematics, Heriot-Watt University, Edinburgh EH14 4AS, UK*
[2] *Department of Surgery, Massachusetts General Hospital, and Shriners Burns Institute, Harvard Medical School, Bldg 1400 W, One Kendall Square, Cambridge MA 02139, USA*
[3] *Department of Mathematics, University of Utah, Salt Lake City, UT 84112, USA*

4.1 Introduction

The various stages of solid tumour formation and progression yield a wide range of pattern formation problems. Broadly speaking, these problems can be divided into two categories: those concerning the overall shape of a tumour, and those concerning internal tumour composition. The former category is important because of its potential use in prognosis: overall tumour morphology has long been known to corrolate with metastatic potential. Recently this connection has been made more precise, via the application of techniques from fractal geometry (Landini and Rippin, 1993, 1996), which shows that the fractal dimension of the tumour boundary is a powerful prognostic indicator. Mathematical modelling of the cellular and biochemical origins of variations in tumour shape have focused primarily on the initial avascular stage of tumour development. This was one of the earliest phases of tumour development to be treated mathematically (Greenspan, 1972), initially under the assumption of spherical symmetry. In the last few years, this work has been extended to study the development of asymmetries. For example, Byrne and Chaplain (1996) and Byrne (1997) studied a model consisting of conservation equations for nutrient and pressure within a tumour, the pressure coming from rapid tumour cell proliferation. Here the tumour edge enters as a free boundary, and the application of spherical harmonic analysis shows that asymmetries develop when the level of cell–cell adhesion is low.

On Growth and Form: Spatio-temporal Pattern Formation in Biology.
Editor Mark A.J. Chaplain, G.D. Singh, J.C. McLachlan

This is consistent with the fact that a reduction in homotypic adhesion is known to be a key ingredient in the onset of metastasis.

Pattern formation in the structure of solid tumours has received much more attention from mathematical modelling than tumour shape. The earliest work in this area focused on the division into a viable rim of proliferating cells around a necrotic core (Greenspan, 1972). Recently, this issue has been studied in detail by Ward and King (1997); their calculations give formulae for the thickness of the viable rim as a function of key model parameters. Many other aspects of internal patterning have also been studied mathematically. For example, the ingrowth of blood vessels into a solid tumour (angiogenesis) involves a complex series of patterning steps, with capillary sprouts advancing into the tumour and then merging to form loops. This has been modelled by Chaplain and coworkers in a series of papers (Chaplain and Sleeman, 1990; Chaplain and Stuart, 1993; Orme and Chaplain, 1996): Orme and Chaplain (1996) have shown how the development of capillary loops depends on an interplay between chemotaxis and haptotaxis of endothelial cells.

In this chapter we focus on two aspects of the internal patterning of tumour cells: the formation of a capsule around solid tumours, and the ability of macrophages to induce tumour heterogeneity.

4.2 Tumour Encapsulation

The presence of a capsule around a tumour is the most significant gross morphological feature determining the clinical outcome. Tumours that are encapsulated (i.e. having a dense band of surrounding connective tissue) have a favourable prognosis and only produce symptoms related to pressure effects on surrounding tissue (Bailey *et al.*, 1995). Such tumours are known as benign. Malignant tumours on the other hand do not have a well circumscribed capsule; the cancerous cells invade neighbouring tissue and are carried far from their primary site by the metastatic cascade (Aznavoorian *et al.*, 1990). Malignant tumours are potentially lethal and may either arise de novo or in existing benign tumours which may be encapsulated. In the latter case the cancerous cells have to disrupt the capsular barrier before spreading further.

Any normal tissue in the body may be viewed simplistically as a collection of different types of cells anchored into position by the presence of intervening extracellular matrix. Among other elements, this extracellular matrix is composed of strands of connective tissue fibres such as collagen, elastin, fibronectin, etc. (William and Gray, 1995). A tumour arises when one of the cells (or sometimes a few) proliferates more rapidly than its neighbours. This aggressive proliferation may be the result of a mutation which encourages division, or one that makes the cell deaf to the inhibitory growth signals from its neighbours (Robbins *et al.*, 1984). In any case the result is a group of cells proliferatively outpacing the neighbouring cells and producing a localised growth - a benign tumour. The pathological hallmark of such a benign tumour is the presence of a dense band of connective tissue around it - the capsule. The capsule is composed chiefly of matrix fibres; we use the term "connective tissue" throughout, following convention. Here we begin by considering the mechanism of capsule formation, using a mathematical formulation of existing ideas on encapsulation. We will use a combination of analytical and numerical techniques to describe the mathematical analogue of encapsulation as a bifurcation from a constant

shape wave to an aggregating wave of connective tissue. The work in this section has been previously reported in Perumpanani *et al.* (1997).

4.2.1 Formulation of the model

We derive a model for the growth of a benign tumour based on a continuum approach, in which $m(x,t)$ and $c(x,t)$ represent the concentrations of the tumour cells and connective tissue respectively. Here x and t are the space and time coordinates. The model studies the averaged behaviour of the tumour cells in the direction of expansion only, and ignores variations in the plane perpendicular to the direction of growth.

In the absence of any surrounding connective tissue we describe the local proliferation of the benign tumour cells by $f(m)$ and the flux of the cells by J_m, say. However, the presence of connective tissue will influence the movement of the benign tumour cells. We describe the effects of connective tissue on the motility of tumour cells by $\theta(c)$, and model the overall flux of the tumour cells by the product $\theta(c)J_m$. We base our model on the "expansive growth hypothesis" for capsule formation, which suggests that the capsule may form by the passive convection of extracellular matrix (ECM) around the tumour as this grows (Berenblum, 1970). This is supported by some pathological evidence, although the alternative "foreign body hypothesis" has some support: this proposes that the capsule forms via an inflammatory response to the tumour (Barr *et al.*, 1988). Based on the expansive growth hypothesis stated earlier, we model the connective tissue flux as being proportional to the flux of the cells, that is, $\theta(c)J_m$. This is the appropriate flux term since the density of connective tissue c is measured per unit volume rather than per cell. In practice there should be a separate saturation term, in addition to $\theta(c)$, representing the limitation on matrix reorganisation potential per cell. However, since we already have a saturation effect via $\theta(c)$, we omit this term for simplicity. Under these assumptions we write the model for benign tumour growth as

$$\frac{\partial m}{\partial t} = f(m) + \frac{\partial}{\partial x}[\theta(c)J_m], \tag{4.1}$$

$$\frac{\partial c}{\partial t} = k\frac{\partial}{\partial x}[c\,\theta(c)J_m]. \tag{4.2}$$

Our approach is based on the prediction of Sherratt and Nowak (1992) that the early growth of a tumour has the form of a travelling wave moving outwards from an initial site of disease into the surrounding normal tissue. The increase in tumour size is primarily driven by cell division; cell movement is just local random motion at the tumour edge. We use simple functional forms of f and J_m which give travelling wave solutions reminiscent of those demonstrated by Sherratt and Nowak (1992). The advantage of such a generic model approach is that the ensuing simplicity allows an analytical appraisal of the equations while retaining the necessary qualitative features. Throughout, we describe the proliferation of tumour cells using the logistic growth model which Vaidya and Alexandro (1982) established as an appropriate model for tumour cell growth. Under an appropriate rescaling of tumour cell density m and time t, this gives $f(m) = m(1-m)$.

We assume that the boundary does not have any significant bearing on the evolution

of the tumour and hence study the case of an infinite domain, which in our numerical simulations is represented by a large finite domain with zero derivative conditions on the boundary. We assume that at time $t = 0$ the tumour cell population is zero except in a small region centred at $x = 0$. We take the initial connective tissue density $c(x, 0)$ to be zero near this region, and a non-zero constant (set arbitrarily to 0.2) away from it. The results of simulations are not sensitive to the details of these initial conditions. To reduce simulation time, we solve only on the region $x \geq 0$, using a symmetry boundary condition at $x = 0$.

4.2.2 Connective tissue waves

We begin by considering equations (4.1) and (4.2) in the simple case of $\theta(c) \equiv 1$; that is, changes in connective tissue density have no effect on cell motility. This case will be relevant during the early stages of tumour growth, in which connective tissue accretion on the surface of the tumour is too low to significantly restrain its expansion. Moreover, study of this simple case gives important mathematical insights into the behaviour for more general forms of $\theta(c)$.

We have solved equations (4.1) and (4.2) numerically with $\theta(c) \equiv 1$ for two different forms for the cell flux. The first case is $J_m = \partial m/\partial x$, in which case equation (4.1) becomes the very well-studied Fisher equation (Murray, 1991). Standard theory shows that for this equation, initial conditions of the form we are using for m evolve to a travelling wave, moving with constant shape and with speed 2. Secondly, we have considered $J_m = m\,\partial m/\partial x$, giving the non-linear Fisher equation, for which our initial conditions evolve to a sharp-front travelling wave, moving with speed $1/\sqrt{2}$ (Sanchez-Garduno and Maini, 1995; Sherratt and Marchant, 1996). Our interest is in the way in which connective tissue is convected by these waves of cell density.

Numerical simulations show that, for both flux terms, the solution for c depends critically on the parameter k, which reflects the strength of connective tissue convection. When k is small, a wave of connective tissue moves in parallel with the wave of tumour cells, with the effect that a constant band of connective tissue is pushed ahead by the growing tumour (Figure 4.1). However, when k increases above a critical value, the form of the solution alters significantly, and the peak in the c-wave increases with time, corresponding to a gradually increasing intensity of the predicted capsule (Figure 4.2).

Before launching into a detailed mathematical analysis of these results, we present a simple intuitive explanation for the change in behaviour. In equation (4.2) with $\theta(c) \equiv 1$, kJ_m is the velocity at which connective tissue is being convected, while a is the speed of the tumour cell wave. When the velocity of the connective tissue wave is slower than the velocity of the cell wave, we expect only a fleeting ripple to be produced in the solution for c. However, when $kJ_m > a$ at some points, the ECM at these points is actually convected faster than the speed at which the cell wave moves, causing a build-up of connective tissue. An analogous physical situation is the difference between the rippling of the surface of a cornfield by wind (small k) and a gust of wind blowing loose strands of hay into a pile (large k). In the analysis that follows, we will show that the bifurcation value of k, at which the c-wave changes from a constant shape wave to an aggregating wave, is indeed $k = a/\max\{J_m\}$.

We will study this case of $\theta(c) \equiv 1$ analytically, with two key objectives – to

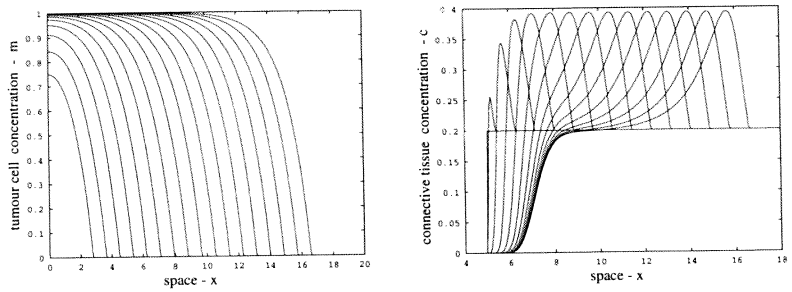

Figure 4.1 Numerical solutions of equations (4.2) with $k = 3.8$, $\theta(c) \equiv 1$, and $J_m = m\,\partial m/\partial x$. In this case the bifurcation value of k is 4. We plot m and c as functions of space at equal intervals of time. Both the m and the c waves eventually evolve into constant shape travelling waves.

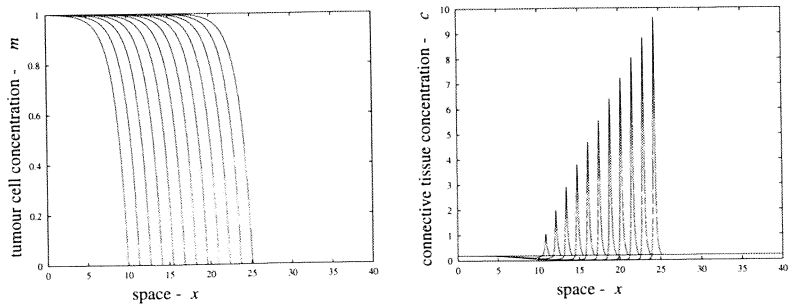

Figure 4.2 Numerical solutions of equations (4.2) with $k = 4.05$, $\theta(c) \equiv 1$, and $J_m = m\,\partial m/\partial x$. In this case the bifurcation value of k is 4. We plot m and c as functions of space at equal intervals of time measuring 1.9. The solution has the form of a constant shape travelling wave for m and an aggregating wave for c.

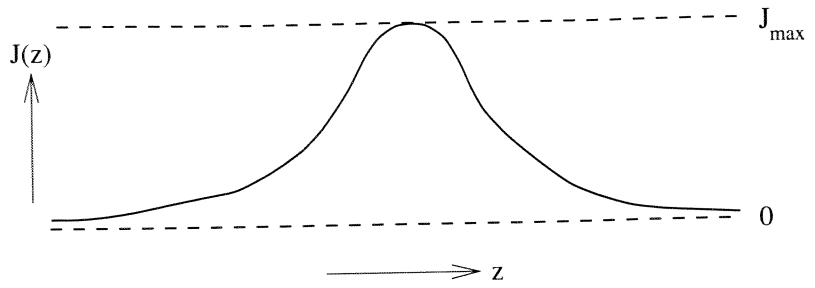

Figure 4.3 The qualitative form of the cell flux $J_m = J(z)$ when cell movement is not hindered by extracellular matrix levels.

determine the value of k at which the c-wave changes form, and the rate at which the peak of c increases when k is above this value. We denote by $M(z)$ the sharp-front travelling wave solution of (4.1) that evolves from our initial conditions; here $z = x - at$ and a is the speed of this cell wave. In the case of the non-linear Fisher equation, a closed-form expression for $M(z)$ exists, but not for the Fisher equation. In either case J_m depends only on M and its derivatives, and can thus be written as a function of z, say $J(z)$.

Rewriting (4.2) in terms of coordinates $\tau = t$ and $z = x - at$ gives

$$\frac{\partial c}{\partial \tau} + [kJ(z) - a]\frac{\partial c}{\partial z} = -kJ'(z)c\,. \tag{4.3}$$

This first-order partial differential equation can be solved exactly using the method of characteristics, and we will use this method to determine the qualitative form of the solution for $c(z, \tau)$ for general $J(.)$. Of course, in practice the solution for $m(x, t)$ only approaches $M(z)$ asymptotically as $t \to \infty$, and thus our solution for c will also only be exact in this limit.

The qualitative form of $J(z)$ is illustrated in Figure 4.3, and is the same for any realistic flux expression. Crucially, we will assume that $J(z) \geq 0$ for all z, with $J(z) \to 0$ as $z \to \pm\infty$, and $J'(z)$ non-zero except at the unique local maximum, at which $J(z) = J_{max}$, say. In the case of non-linear cellular diffusion, $J(z)$ is identically zero for sufficiently large z, since the m-wave is of sharp-front type, but this will not be significant in our calculations.

The characteristics of (4.3) are given by solving

$$d\tau = \frac{dz}{kJ(z) - a} = \frac{-dc}{kJ'(z)c}\,,$$

which gives the two characteristic functions

$$\mathcal{C}_1(c, z) = c/c_{tw}(z) \quad \text{and} \quad \mathcal{C}_2(\tau, z) = \tau - G(z)$$

$$\text{where} \quad c_{tw}(z) = 1/[a - kJ(z)] \quad \text{and} \quad G(z) = -\int c_{tw}(z)\,dz\,.$$

Thus the solution for c is given by eliminating the parameter θ, say, from

$$\frac{c}{c_{tw}(z)} = \frac{c_0(\theta)}{c_{tw}(\theta)} \quad \text{and} \quad G(z) - \tau = G(\theta)\,. \tag{4.4}$$

Here $c_0(x) \equiv c(x, t = 0)$. The key determinant of the form of this solution is the sign of $kJ_{max} - a$. If this expression is negative then $\mathcal{C}_1(c, z)$ is finite for all z, so that a possible solution is $c(z, \tau) = c_{tw}(z)$, independent of τ. This is a travelling wave solution for c and it is straightforward to show, using the method of characteristics, that all bounded initial conditions evolve to this solution, multiplied by $c_0(\theta)$, as $\tau \to \infty$.

The case $kJ_{max} > a$ is more complicated, however (Figure 4.4). Then $c_{tw}(z)$ has the qualitative form illustrated in Figure 4.4b, with infinities at the points, z_1 and z_2 say $(z_1 < z_2)$, at which $kJ(z) = a$. Thus the solution for c cannot be of travelling wave form, and must be determined from (4.4). Integrating c_{tw} shows that $G(z)$ has the qualitative form illustrated in Figure 4.4c, also with infinities at z_1 and z_2. In order to use the solution (4.4), we require the parameter θ, which is given by $\theta(z, \tau) = G^{-1}[G(z) - \tau]$; here G^{-1} denotes the local inverse. The qualitative form of θ as a function of z at successively increasing τ is illustrated in Figure 4.4d. Crucially $\theta(z_1, \tau) \equiv z_1$ and $\theta(z_2, \tau) \equiv z_2$.

For simplicity, we begin by considering the case $c_0(x) \equiv 1$, so that (4.4) implies $c(z, \tau) = c_{tw}(z)/c_{tw}(\theta(z, \tau))$. The qualitative form of $c_{tw}(\theta)$ as a function of z at increasing τ is illustrated in Figure 4.4e, and compared to $c_{tw}(z)$. However, from these sketches alone it is not possible to determine the form of the ratio $c_{tw}(z)/c_{tw}(\theta)$, since the behaviour near $z = z_1$ and $z = z_2$ is not clear, and requires detailed analysis.

For z close to z_1, $kJ(z) - a \approx \lambda(z - z_1)$, where $\lambda = kJ'(z_1)$; our assumption that $J'(z) \neq 0$, except at the unique maximum, implies that $\lambda > 0$. Thus to leading order near $z = z_1$,

$$
\begin{aligned}
G(z) &= \lambda^{-1} \log|z - z_1| \\
\Rightarrow G^{-1}(\xi) &= z_1 + \exp(\lambda\xi) \cdot \operatorname{sign}(z - z_1) \\
\Rightarrow \theta &\equiv G^{-1}[G(z) - \tau] \\
&= z_1 + \exp\left\{\lambda\left[\lambda^{-1} \log|z - z_1| - \tau\right]\right\} \cdot \operatorname{sign}(z - z_1) \\
&= z_1 + (z - z_1)e^{-\lambda\tau} \\
\Rightarrow c(z, \tau) &\equiv c_{tw}(z)/c_{tw}(\theta) \\
&= \left[\frac{1}{-\lambda(z - z_1)}\right]\left[\frac{1}{-\lambda(\theta - z_1)}\right]^{-1} \\
&= e^{-\lambda\tau}.
\end{aligned}
$$

Thus the solution for c near $z = z_1$ decreases to zero exponentially in time. Moreover, this calculation is valid whenever both θ and z are close to z_1, so that the region in which c is close to zero remains finite as τ increases.

A similar calculation shows that $c(z_2, \tau) = e^{+\mu\tau}$, where $\mu = -kJ'(z_2) > 0$, so that c has a maximum at $z = z_2$, whose height increases exponentially with time. However, the width of the peak decreases at a corresponding exponential rate, so that the net amount of connective tissue within this peak ($\propto$ its area) is roughly constant. This is because the calculation of the solution form near $z = z_2$ is only valid provided $1 \gg |\theta - z_2| = |z - z_2|e^{\mu\tau}$; that is, provided $|z - z_2| \ll e^{-\mu\tau}$.

Putting these various calculations together implies that the qualitative form of $c(z, \tau)$ when $kJ_{max} > a$ and $c_0(x) \equiv 1$ is as illustrated in Figure 4.4e. There is a peak in c at $z = z_1$, whose height and width increase and decrease exponentially in

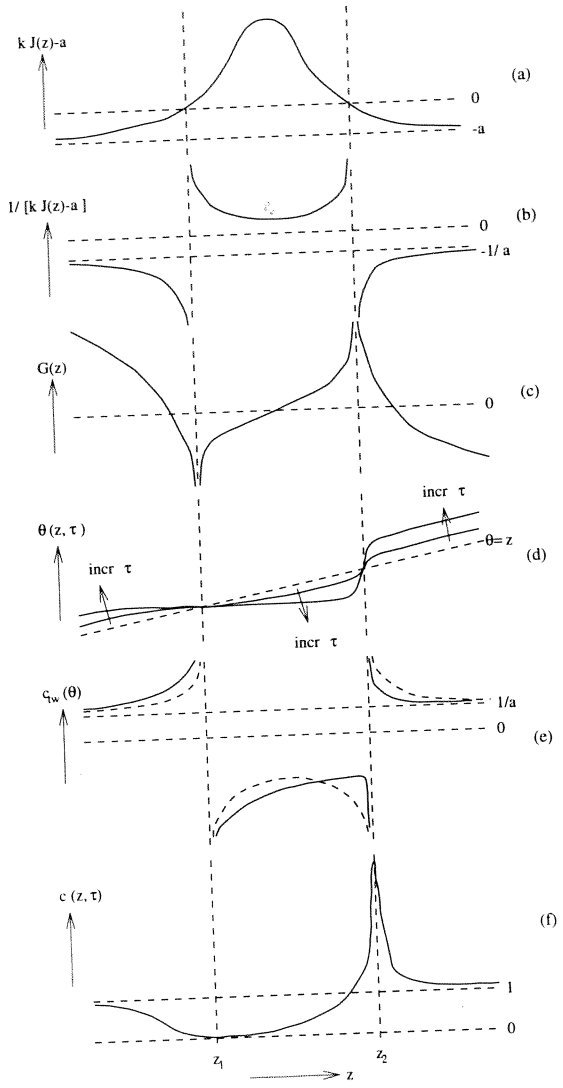

Figure 4.4 The qualitative form of the various functions involved in the solution of (2) using the method of characteristics. The explanation for these forms is given in the main text. (a) illustrates the form of $kJ(z) - a$. (b) shows $1/[kJ(z) - a]$, and (c) shows its integral, $G(z)$. (d) illustrates the form of $\theta(z, \tau)$. (e) shows $c_{tw}(\theta)$ (full curve) compared with $c_{tw}(z)$ (dashed curve). Finally, (f) shows the ratio $c_{tw}(z)/c_{tw}(\theta)$ at one value of τ

time, respectively, and a trough in c centred at $z = z_1$, whose width increases with time.

For illustration, we consider the particular case of non-linear cellular diffusion, $J_m = m\,\partial m/\partial x$. In this case, standard analysis (Sanchez-Garduno and Maini, 1995) shows that the travelling wave solution for cell density that evolves from our initial conditions has the form

$$\begin{aligned} M(z) &= \begin{cases} 1 - \exp\left[\frac{z-z_c}{\sqrt{2}}\right], & z < z_c \\ 0, & z > z_c \end{cases} \\ \Rightarrow J(z) &= \begin{cases} \frac{1}{\sqrt{2}}\left(\exp\left[\frac{z-z_c}{\sqrt{2}}\right] - \exp\left[(z-z_c)\right]\right), & z < z_c \\ 0, & z > z_c\,. \end{cases} \end{aligned}$$

Solving the equation $kJ(z) = 1/\sqrt{2}$ shows that

$$z_1,\, z_2 = \sqrt{2}\log\left(\frac{1 \pm \sqrt{1 - 4/k}}{2}\right).$$

When $k < 4$ these roots are complex, and the travelling wave solution for c exists and is the long-term solution: this solution is

$$c(z) = \begin{cases} \dfrac{\sqrt{2}}{\sqrt{2} - k\sqrt{2}\exp\left(\dfrac{z-z_c}{\sqrt{2}}\right) + k\sqrt{2}\exp(\sqrt{2}(z-z_c))}, & z < z_c \\ 1, & z > z_c\,. \end{cases}$$

(for $c_0(x) \equiv 1$). When $k > 4$, however, the solution for c has the aggregating waveform described above; straightforward calculation shows that

$$\begin{aligned} \lambda &= (k/4)\sqrt{1 - 4/k}\left[1 - \sqrt{1 - 4/k}\right] \\ \mu &= (k/4)\sqrt{1 - 4/k}\left[1 + \sqrt{1 - 4/k}\right] \end{aligned}$$

These results are confirmed by numerical simulations of (4.1); the example of $k = 4.05$ is illustrated in Figure 4.2.

When $c_0(x)$ is not constant, the solution for c is given by multiplying $c_{tw}(z)/c_{tw}(\theta)$ by $c_0(\theta)$. Moreover, this solution is then only exactly valid when $m(x, 0)$ is exactly in travelling wave shape, although since m evolves to the travelling wave shape quite quickly (Figures 4.1a and 4.2a), we expect the analysis to determine the key qualitative features of the solution for c. For the step function form of $c_0(.)$, this multiplication by $c_0(\theta)$ has the effect of removing the trough in the solution for $c(z, \tau)$, although the growing peak remains.

This analysis applies only when $\theta(.) \equiv 1$, implying that the extracellular matrix density does not affect cell movement. Allowing $\theta(.)$ to vary is extremely difficult because the equations no longer decouple, so the method used above cannot be applied. However, numerical simulations suggest that provided the variation in $\theta(.)$ is not too great, the qualitative behaviour of the solutions remains similar to when $\theta(.)$ is constant.

4.2.3 Extension to model transcapsular spread

The modelling in this section has demonstrated a novel bifurcation of a travelling wave into a more general waveform, not of constant shape. It also presents a succinct model for the accretion of connective tissue on the surface of a growing tumour.

Equations (4.1) and (4.2) are of course extremely simplistic and neglect a great many features of real tumour growth. A tumour cell interacts with the connective tissue in several ways, depending on the range of mutations it has undergone (Aznavoorian *et al.*, 1990). Benign tumour cells merely advect and compress surrounding connective tissue, thereby causing encapsulation (Carter *et al.*, 1985). Further mutations can make the cells invasive. These mutations can cause the cells to produce large amounts of proteases leading to digestion of the connective tissue, or can make the cells sensitive to connective tissue gradients (chemotaxis and haptotaxis) (Aznavoorian *et al.*, 1990) or alter their adhesiveness (Parsons, 1993). These phenotypic changes in a cell allow it to invade neighbouring tissue and to be carried away far from its primary site (Stetler-Stevenson *et al.*, 1993).

When malignant transformation occurs in an encapsulated benign tumour, the capsule is at first disrupted by the action of proteases and the cells can then escape into the surrounding tissue (Carter *et al.*, 1985). Clinically this transcapsular spread represents a crucially important point in the evolution of the tumour. Before transcapsular spread the prognosis for a malignant tumour is favourable, since the tumour can be completely removed by surgery. However, once the capsule has been disrupted, more aggressive forms of surgery (e.g. wide dissection) will be required, often in combination with other forms of treatment such as chemotherapy or radiotherapy. More importantly, the final outcome of treatment in patients with transcapsular spread compares poorly with tumours that are confined by the capsule (Bailey *et al.*, 1995).

We conclude this section by describing the results of simulations of an improved version of equations (4.1) and (4.2) which incorporates some of the features discussed above. The model includes a study of the behaviour of normal cells. Tumour cells differ from normal cells both in their local behaviour (e.g. the loss of contact inhibition and the ability to produce proteases) and in their spatial behaviour (e.g. enhanced chemokinesis, chemotaxis and haptotaxis). Here we describe the consequence of a mutation resulting in the loss of contact inhibition and another resulting in the production of a protease by the cancer cells.

When a malignant tumour produces proteases (e.g. matrix metalloproteases), this typically occurs at the growing edge of the tumour which is in contact with the surrounding connective tissue (Xie *et al.*, 1994). The body produces other proteins called antiproteases that have the ability to neutralise the effects of the proteases. Also, being small biochemicals, proteases can diffuse into the surrounding tissue. This results in the digestion of surrounding connective tissue, providing a mechanism for the possible disruption of the capsule. To study the occurrence of such capsular disruption we expand equation (4.2) to incorporate the dynamics of the proteases. The new model has the form

$$\frac{\partial n}{\partial t} = k_1 n(k_2 - n - m) + k_3 \frac{\partial}{\partial x}\left[n \frac{\partial n}{\partial x}\right], \tag{4.5}$$

$$\frac{\partial m}{\partial t} = k_4 m(k_5 - n - m) + k_6 \frac{\partial}{\partial x}\left[m \frac{\partial m}{\partial x}\right], \tag{4.6}$$

$$\frac{\partial c}{\partial t} = -k_7 pc + k \frac{\partial}{\partial x}\left[cm \frac{\partial m}{\partial x}\right], \tag{4.7}$$

$$\frac{\partial p}{\partial t} = k_8 uc - k_9 p - k_{10} up - k_{11} pc + k_{12} \frac{\partial^2 p}{\partial x^2}. \tag{4.8}$$

where $n(x,t)$ is the concentration of the normal cells and $p(x,t)$ is the concentration of the protease. Here the k_i's are all positive constants. k_1 and k_4 represent the linear growth rates of the normal cells and the tumour cells, and k_2 and k_5 their maximum carrying capacities. Thus the difference $k_5 - k_2$ is a measure of the loss of contact inhibition. k_3 and k_6 represent the effective diffusion coefficients of the normal cells and tumour cells. The interpretation of the various terms in equations (4.7) and (4.8) are as follows:

$-k_7 pc$	represents the degradation of connective tissue by the protease
$k_8 uc$	represents the production of the protease at the interface of the tumour and the surrounding tissue
$-k_9 p$	models the natural degradation of the protease
$-k_{10} up$ and $-k_{11} pc$	represent the neutralisation of the protease by the action of antiproteases.

The constant k_{12} is the diffusion coefficient of the protease.

Figure 4.5 illustrates a typical numerical solution of the improved model (4.8). In this simulation, we begin solution with $k_8 = 0$; that is, no protease is produced. This results in the formation of a capsule in a manner very reminiscent of the solutions discussed in Section 4.2.2. But there is also the dynamics of the normal cell population to consider; the receding wave of these cells corresponds to their out-competition by the tumour cells. Partway through the simulation, we alter k_8 to have a positive value, which crudely simulates the occurrence of a mutation resulting in the production of protease by the tumour cells. Once this mutation has occurred and protease production starts, the capsule is disrupted, as shown by the absence of increasing waves of c. In this second part of the solution, the cancer cells can spread unhindered by the capsule.

The simulation illustrated in Figure 4.5 has two key implications. Firstly, it demonstrates capsule formation via the mechanism described earlier in the section, but in an enlarged and somewhat more realistic model, adding to the credibility of this mechanism. Secondly, it shows that the mechanism is consistent with postulated methods of capsule disruption. However, it must be stressed that for cancer cells to spread aggressively, they need additional mechanisms of motility such as chemotaxis and haptotaxis, and alterations in adhesivity. Work is currently in progress in our group to understand the contribution of these various interactions to cancer invasion.

4.3 Macrophage Induction of Tumour Heterogeneity

Macrophages form an important part of the immune response to cancer. They are the mature form in tissue of a type of white blood cell known as a monocyte, and are

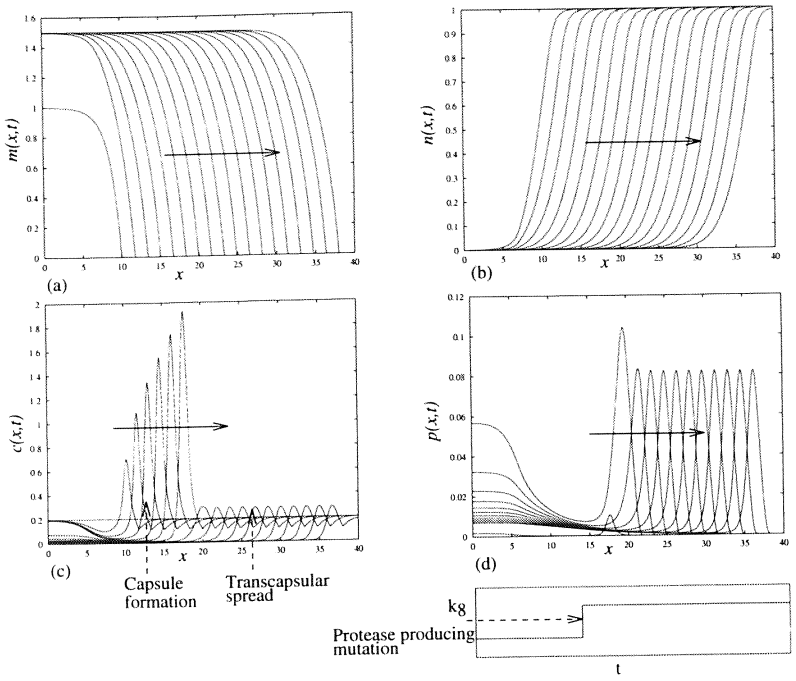

Figure 4.5 Numerical solution of equation (4.8) showing the replacement of normal tissue (b) by tumour cells (a) and an incipient capsule (c) being degraded by the action of a protease (d) produced by a mutation in the tumour cell. The parameter values used in this simulation are $k_1 = 5$, $k_2 = 1$, $k_3 = 1$, $k = 5$, $k_4 = 1$, $k_5 = 1.5$, $k_6 = 1$, $k_7 = 5$, $k = 5$, $k_9 = 3.1$, $k_{10} = 0.1$, $k_{11} = 0.1$, $k_{12} = 0.1$. The arrows show the direction of increasing time.

recruited to tumour sites by attracting gradients of chemicals produced by tumour cells. This recruitment can be very effective: for example, in many cases of breast carcinoma, macrophages constitute over 50% of the total cell mass (O'Sullivan and Lewis, 1994). The role of macrophages within tumours is complex. They are known to selectively kill tumour cells (Mantovani *et al.*, 1992) but they can also promote tumour growth by encouraging vascularisation (Lewis *et al.*, 1995). These various processes will be explained more fully later in the chapter; for more detailed biological reviews, see Hamilton and Adams (1987), Esgro *et al.* (1990) and Mantovani (1990).

Here we consider the effect of macrophage-mediated killing of tumour cells during the early, avascular stage of tumour growth. This process is initiated when a cell in the tissue undergoes a mutation, giving it a proliferative advantage over its normal counterparts (Weinberg, 1989); mathematical models for this process are given in Wheldon (1975) and Sherratt and Nowak (1992). The avascular phase of growth terminates because of the limited rate at which nutrients can diffuse into a solid tumour (Groebe and Mueller-Klieser, 1991) and thereafter the tumour becomes quiescent; this diffusion-limited cessation of growth was the first area of tumour biology to be modelled mathematically (Burton, 1966; Greenspan, 1972; Adam, 1986) and recent modelling has clarified the effects of tumour shape on the process (Byrne and Chaplain, 1995; Ward and King, 1997). Tumour growth is then resumed via the onset of angiogenesis (Folkman, 1995) in which tumours acquire their own blood supply, leading to unconstrained (and potentially lethal) growth; for models of the angiogenic process, see Chaplain and Sleeman (1990); Chaplain and Stuart (1993); Anderson and Chaplain (1998). Subsequent metastasis, leading to secondary tumours, requires the development of invasive tumour cell phenotypes; for modelling of tumour invasion, see Perumpanani *et al.* (1996).

Previous mathematical models of tumour immunology fall into two main categories, using either generic representations of the immune response (Adam, 1993; Albert *et al.*, 1980; Hiernaux and Lefever, 1988; Sherratt and Nowak, 1992) or detailed models focusing on particular aspects of immune cell–tumour cell interactions (Kuznetsov *et al.*, 1993; Kuznetsov, 1996; Adam and Bellomo, 1996). Our approach falls in between these categories of model: we focus specifically on macrophages, and use equations that are based at least qualitatively on known details of macrophage–tumour interactions; however, we keep our modelling sufficiently simple that we can consider the effects of macrophages within the context of a tumour that is growing in space. The work presented in this section has been previously reported in Owen and Sherratt (1997, 1998a, b).

4.3.1 Model development

Our model restricts attention to the interactions between mutant cells, normal tissue, macrophages, and their chemical regulators. We make the simplifying assumption that there is a single chemical regulator responsible for activation of macrophages, control of their proliferation, and stimulation of their influx from the bloodstream. In reality, many different chemicals are involved, including tumour necrosis factor (Mace *et al.*, 1988), macrophage colony stimulating factor (Sampson-Johannes and Carlino, 1988), and members of the monocyte chemotactic protein family (Bottazzi *et al.*, 1983; van Damme *et al.*, 1992); however, all these regulators derive primarily from mutant cells,

and can be treated together to a first approximation.

Activation and inhibition of mutant and normal cell growth are not included in our model; instead we represent the proliferative advantage of mutant cells in terms of an increased basic growth rate. Thus the variables we consider are the densities of macrophages, $l(\mathbf{x},t)$; mutant cells, $m(\mathbf{x},t)$; normal cells, $n(\mathbf{x},t)$; macrophage–mutant cell complexes, $c(\mathbf{x},t)$; and the concentration of the chemical regulator, $f(\mathbf{x},t)$. In the following sections we will outline the assumptions and interactions relevant to each species, and give mathematical descriptions in terms of differential equations.

Macrophages destroy tumour cells by binding to form a complex and then lysing the mutant cell; direct cell–cell contact is an essential part of this process (Jonjic *et al.*, 1992). Quiescent macrophages must be biochemically activated before complex formation and lysis are possible (Hamilton and Adams, 1987; Mantovani, 1990). We assume that the rate of complex formation is linear with respect to chemical concentration, and macrophage and tumour cell densities. In addition we assume that the complex returns viable macrophages after lysis of the mutant cell (Esgro *et al.*, 1990). Note that the source of regulators is mutant cells. Schematically this can be represented in the following form:

$$f + l + m \xrightarrow{k_1} c + f \qquad c \xrightarrow{k_2} l + \text{debris}.$$

Here k_1 and k_2 are positive constants. It is important to stress that there is no definitive experimental data on the details of this tumour cell destruction; we have considered various alternative formulations for this process, such as separating the activation and complex formation steps, but such changes do not significantly alter the qualitative model behaviour.

The remaining assumptions that we make with regard to macrophages are (i) they have spatially random motion combined with movement up gradients in the concentration of chemical regulator; (ii) they proliferate only in the presence of the chemical regulator (Bottazzi *et al.*, 1990), and such proliferation increases linearly with the concentration; (iii) their proliferation is limited by the crowding effect of all cell types; (iv) there is an influx from capillaries, which, due to chemotaxis, increases linearly with regulator concentration; and (v) they die with some constant rate per cell. In the absence of chemical regulator, the normal background level of tissue macrophages is maintained by a constant influx, at a rate denoted by I.

We use a term for proliferation of macrophages of the form

$$\text{(chemical concentration)} \times \text{(macrophage density)} \times \text{(crowding term)}.$$

The most common representation of crowding effects on cell division is the logistic term, $r(x) = (k - x)$, which has been used in modelling a wide range of biological systems (Fisher, 1937; Sherratt and Murray, 1991). In this case it is inappropriate, since the logistic crowding term can be negative, which does not make sense when it is multiplied by the chemical concentration – macrophage death should not be promoted. Therefore we use the term $r(x) = (N + N_e)/(N + x)$, where N_e is the equilibrium cell density in normal tissue and N is a measure of crowding response. There is no particular significance in this choice of functional form; in the absence of detailed biological data, only the qualitative form of the function is known.

Combining these terms gives the following conservation equation for macrophages:

$$\frac{\partial l}{\partial t} = \overbrace{D_l \nabla^2 l}^{\text{cell migration}} + \overbrace{\frac{\alpha f l(N+N_e)}{N+l+m+n}}^{\text{proliferation}} + \overbrace{I(1+\sigma f)}^{\text{influx}} - \overbrace{k_1 f l m + k_2 c}^{\text{lysis}} - \overbrace{\delta_l l}^{\text{death}} . \tag{4.9}$$

Most tumours arise initially from a mutation that affects the control of cell division, giving the mutant cell a proliferative advantage over its peers (Weinberg, 1989). Such mutations have been the subject of previous detailed models (Wheldon, 1975; Sherratt and Nowak, 1992), but here our focus is on the role of macrophages during the early stages of tumour growth, and thus we use a very simple model. Specifically, we assume that the dynamics of mutant and normal cells are alike except for the removal of mutant cells by macrophages, and a scaling of the mutant cell growth rate by $\xi > 1$ to model their proliferative advantage. We use the same crowding term as discussed above, and a growth rate in normal tissue of δ, balanced by an equal rate of cell death, so that combining these elements with diffusion to simulate random cell migration gives the following conservation equations for mutant and normal cells:

$$\begin{aligned} \frac{\partial m}{\partial t} &= \overbrace{D_m \nabla^2 m}^{\text{cell migration}} + \overbrace{\frac{\xi \delta m(N+N_e)}{N+l+m+n}}^{\text{proliferation}} - \overbrace{\delta m}^{\text{death}} - \overbrace{k_1 f l m}^{\text{lysis}} \\ \frac{\partial n}{\partial t} &= D_n \nabla^2 n + \frac{\delta n(N+N_e)}{N+l+m+n} - \delta n. \end{aligned} \tag{4.10}$$

Chemotaxis, macrophage proliferation, and mutant cell lysis are the important interactions considered in this model, and all are stimulated by chemicals produced by mutant cells, which we are representing as a single generic regulator $f(\mathbf{x}, t)$, whose sole source is mutant cells. We assume a constant secretion rate β per unit of mutant cell density, and a linear natural decay with rate δ_f. The complex density is also assumed to decay linearly, with rate δ_c. Including random motion and the binding and lysis terms discussed above completes the derivation of our model:

$$\begin{aligned} \frac{\partial f}{\partial t} &= \overbrace{D_f \nabla^2 f}^{\text{diffusion}} + \overbrace{\beta m}^{\text{prod}^n} - \overbrace{\delta_f f}^{\text{decay}} \\ \frac{\partial c}{\partial t} &= \overbrace{D_c \nabla^2 c}^{\text{migration}} + \overbrace{k_1 f l m - k_2 c}^{\text{lysis}} - \overbrace{\delta_c c}^{\text{death}} . \end{aligned} \tag{4.11}$$

Equations (4.9) to (4.11) are non-dimensionalised using the following rescalings, where L is half a typical cell length, and f_0 is a typical concentration of chemical regulator:

$$t^* = \delta t, \; x^* = x/L, \quad l^* = l/N_e, \; m^* = m/N_e, \; n^* = n/N_e, \; c^* = c/N_e, \quad f^* = f/f_0,$$

$$D_l^* = \frac{D_l}{\delta L^2}, \quad D_m^* = \frac{D_m}{\delta L^2}, \quad D_n^* = \frac{D_n}{\delta L^2}, \quad D_f^* = \frac{D_f}{\delta L^2}, \quad D_c^* = \frac{D_c}{\delta L^2},$$

$$\alpha^* = \alpha f_0/\delta, \quad N^* = N/N_e, \quad I^* = I/(N_e \delta), \quad \sigma^* = f_0 \sigma, \quad k_1^* = k_1 f_0 N_e/\delta,$$

$$k_2^* = k_2/\delta, \quad \delta_l^* = \delta_l/\delta, \quad \delta_f^* = \delta_f/\delta, \quad \delta_c^* = \delta_c/\delta, \quad \beta^* = \beta N_e/(f_0\delta).$$

Recall that N_e is the equilibrium cell density in normal tissue. Applying these rescalings, and dropping the asterisks for notational simplicity, gives

$$\frac{\partial l}{\partial t} = D_l\nabla^2 l + \frac{\alpha f l(N+1)}{N+l+m+n} + I(1+\sigma f) - k_1 f l m + k_2 c - \delta_l l \tag{4.12}$$

$$\frac{\partial m}{\partial t} = D_m\nabla^2 m + \frac{\xi m(N+1)}{N+l+m+n} - m - k_1 f l m \tag{4.13}$$

$$\frac{\partial n}{\partial t} = D_n\nabla^2 n + \frac{n(N+1)}{N+l+m+n} - n \tag{4.14}$$

$$\frac{\partial f}{\partial t} = D_f\nabla^2 f + \beta m - \delta_f f \tag{4.15}$$

$$\frac{\partial c}{\partial t} = D_c\nabla^2 c + k_1 f l m - k_2 c - \delta_c c. \tag{4.16}$$

The experimental data available for parameter estimation is limited, but enables order of magnitude estimates to be obtained for most of the parameters, and details of this are given in Owen and Sherratt (1998a) for the kinetic parameters, and in Owen and Sherratt (1998b) for motility parameters.

4.3.2 Spatially independent solutions

Although we are primarily concerned with spatially varying solutions, as an essential precursor to this work, we discuss solutions of the spatially homogeneous system given by setting $D_l = D_m = D_n = D_f = D_c = 0$. In the resulting system of ordinary differential equations, there are four types of steady state to consider. The first two are somewhat trivial: a macrophage-only state $l = I/\delta_l$, $m = n = f = c = 0$, and the normal tissue state, consisting of normal cells and macrophages, $l = I/\delta_l$, $m = 0$, $n = 1 - I/\delta_l$, $f = c = 0$. Straightforward linear stability analysis shows that both these steady states are unstable to the introduction of mutant cells.

The third type of steady state is that of a tumour with no normal cells remaining, denoted the mutant-only steady state, and the fourth steady state is of mixed type, with all cell species coexisting. Real tumours certainly contain a variety of cell types (Mantovani, 1990), and other models (Wheldon, 1975; Sherratt and Nowak, 1992) also predict this type of solution. If the growth advantage of mutant cells is too high, coexistence is not possible, and steady states of this type cannot exist. Figure 4.6 illustrates the way in which these last two steady states change with σ, the macrophage influx parameter. We have identified a number of bifurcation points, at which the number and stability of steady states change. This is discussed in some detail in Owen and Sherratt (1998a); for the purposes of this chapter the key result is that, with respect to homogeneous perturbations, at least one tumour steady state is stable, and that for realistic parameter ranges there is only a very small region of parameter space in which both coexistence and mutant-only steady states are stable.

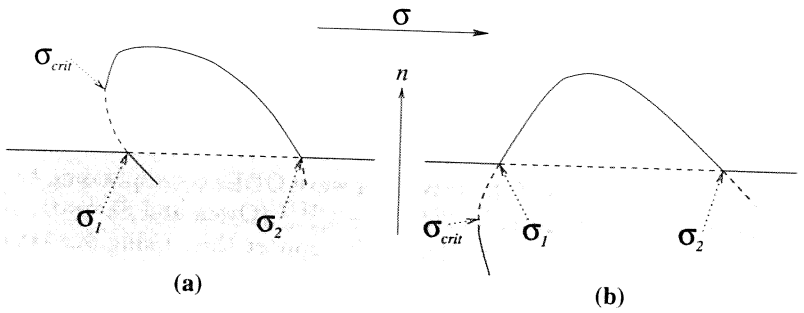

Figure 4.6 Schematic representation of th bifurcation structures for the homogeneous tumour steady states of the dimensionless model (4.16). Solid lines indicate stability, dashed lines instability. The bifurcation parameter σ is the measure of the increase in macrophage influx from the bloodstream in response to chemoattractants secreted by tumour cells.

Numerical simulations of the ordinary differential equation model given by setting $D_l = D_m = D_n = D_f = D_c = 0$ suggest that when only one steady state is locally stable, it is also globally stable for positive solutions; in the small regions of parameter space where two tumour steady states are both locally stable, solutions evolve to one or other of these, depending on initial conditions. In particular, this implies that introduction of a small mutant cell density to the normal tissue state causes the solution to evolve to a tumour steady state. This occurs despite the presence of cytotoxic macrophages, because the macrophage immune response is second order in the density of mutant cells. By this we mean that as well as having an explicit dependence on the mutant cell density m, the immune response term $-k_1 flm$ also depends on the concentration of chemical regulator f, whose production rate is itself dependent on the mutant cell density.

4.3.3 Wave front solutions and spatial patterns

Real tumours in vivo are nearly always spatially heterogeneous, often with no apparent order whatsoever. This should be no surprise given the varied environment in which tumours grow, and the wide variety of interactions with different cell types and tissue structures. Such spatial variations can arise from a variety of biological mechanisms, which include convection and mechanical stress due to movement of the underlying tissue structures, and heterogeneities in the underlying tissue itself. These features do not relate specifically to the macrophage–tumour interaction, and are not considered in our model, although they may be very significant. However, we will show that spatial variations can arise simply as a consequence of cell movement and chemical diffusion, within the context of the macrophage–tumour interaction. In this section we discuss the implications of purely random motility of cells and diffusion of the chemical regulator; we also demonstrate the existence of travelling wave solutions, and the possibility of spatial patterning within the tumour.

We are concerned with the evolution of model solutions following a spatially localised introduction of mutant cells to an infinite domain on which the system is at the normal tissue steady state. In a wide range of numerical simulations, we have found

that provided the chemical diffusion coefficient D_f is sufficiently small, this results in a travelling wave solution originating from the site of mutation, with either the coexistence or mutant-only tumour steady state behind the wave, depending on the kinetic parameters. Figure 4.7 illustrates this simulation, with parameters such that the stable homogeneous steady state, and hence the state behind the wave, is of coexistence type. Linear analysis of the travelling wave ODEs corresponding to (4.16) suggests that the wave speed is given by $2[D_m(\xi-1)]^{1/2}$ (Owen and Sherratt, 1998b), and extensive numerical simulations of the PDEs support this. Using our estimated parameter values, this gives a dimensional wave speed of the order of 10^{-10}ms^{-1}, indicating that it would take about 100 days for a tumour to grow to a size of 1mm.

These results show that the macrophage population has no effect on the speed of tumour growth; however, the macrophages do have a significant effect on tumour composition, because of their effect on the homogeneous steady states. Moreover, when the chemical diffusion coefficient D_f increases above a critical value, numerical simulations of the model predict a much more significant effect on tumour composition, with a spatial pattern developing behind the advancing wavefront, as illustrated in Figure 4.8. Note that the pattern is stationary behind the wave, growing in extent but not changing in form or location. Such regular patterns are not observed in the stochastic inhomogeneous environment of a real tumour, but their observation in model solutions suggests that the macrophage–tumour interaction may be a first step towards the more irregular spatial inhomogeneities seen in the real situation.

This pattern formation is an example of a Turing mechanism (Murray, 1991). However, there is no prepattern involved: in this case the mutant cells are the local activator, and the chemical regulator is the long-range inhibitor. Thus, an intuitive explanation for this spatial instability, illustrated in Figure 4.9 is that given a local perturbation increasing the density of mutant cells, chemical regulator production will also increase locally. Then if the chemical diffuses fast enough, it will act non-locally to activate macrophages to the tumoricidal state and to stimulate an additional influx of macrophages. This will suppress non-local mutant cell growth, while enhancing local mutant cell growth, due to the relative suppression of local macrophage activation, so the original perturbation will grow in time. Thus it is the inclusion of chemical diffusion, which occurs at a much faster rate than random cell migration, that is responsible for this diffusion-driven instability. The diffusion coefficient D_f for the chemical regulator is expected to be substantially larger than the random motility coefficients for cells, but we are not aware of data enabling precise values to be calculated. Such data would in fact be relatively easy to obtain via in vitro experiments, and our results suggest this would be a valuable line of experimental investigation.

We analyse the patterning phenomenon by linearising the model (4.16) about the stable homogeneous steady state. A general perturbation can then be expressed as a linear combination of spatial modes, and so substituting solutions proportional to $e^{i\kappa x+\lambda t}$ into the linearised equations and looking for non-trivial solutions gives the dispersion relation for the real part of λ (i.e. the growth rate) as a function of wave number κ. The homogeneous steady state is then stable to all spatial perturbations if $\text{Re}(\lambda)<0$ for all $\kappa\in\text{R}$, whereas if $\text{Re}(\lambda)>0$ for some κ then the mode corresponding to that wave number will grow exponentially in time, destabilising the homogeneous steady state.

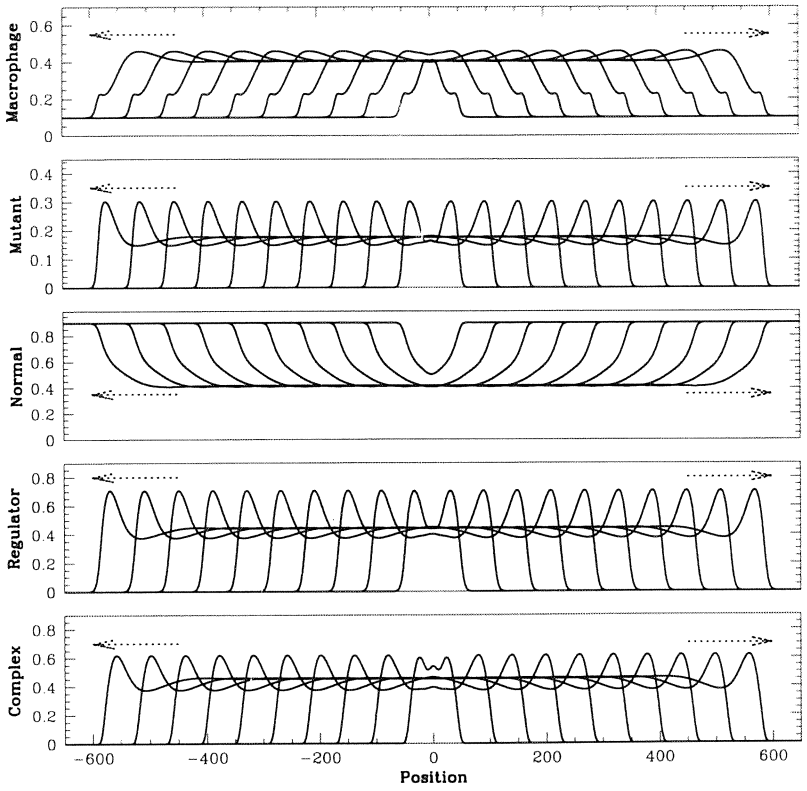

Figure 4.7 Numerical simulation in one dimension of the dimensionless model (4.16), showing the evolution from a localised mutation at the centre. The initial conditions were the normal tissue steady state $l = 0.1, m = 0, n = 0.9, f = 0, c = 0$ on the whole domain, apart from the mutation $l = 0, m = 1, n = 0, f = 0, c = 0$ for $-0.5 < x < 0.5$. A travelling wave is established as the tumour grows, with the composition behind the wave front that of the homogeneous stable steady state, which is dependent on the kinetic parameters. The parameters are: $D_l = D_m = D_n = 5,\ D_f = 30,\ D_c = 2.5, \alpha = 0.01,\ \beta = 5.0,\ \delta_c = 0.5,\ \delta_f = 2.0,\ \delta_l = 0.1,\ N = 1,\ I = 0.01,\ k_1 = 10.0,\ k_2 = 0.2,\ \sigma = 58,\ \xi = 2.8.$

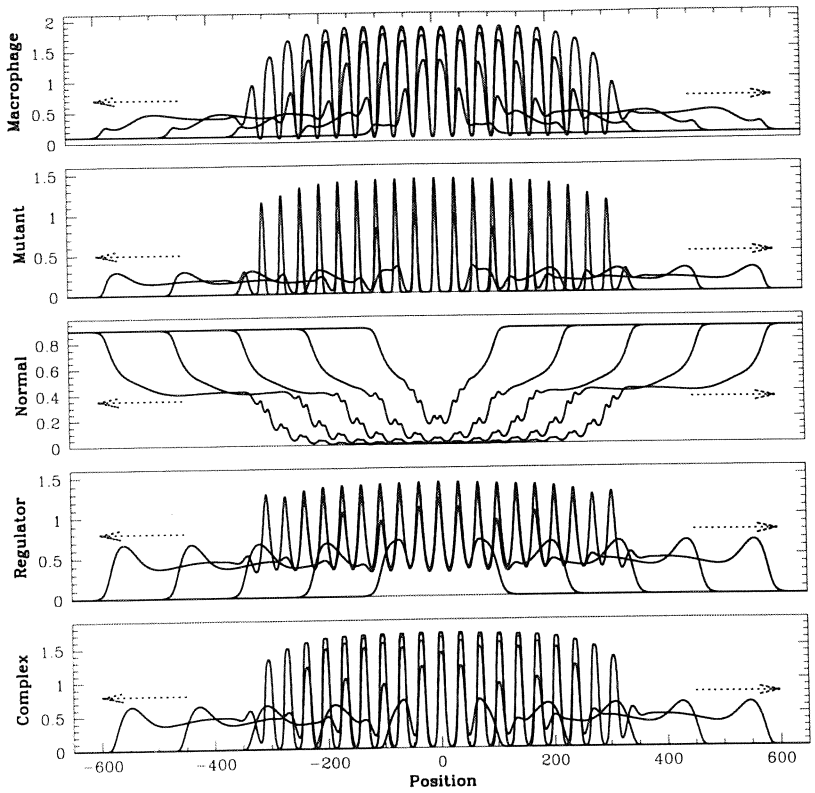

Figure 4.8 Numerical simulation in one dimension of the model (4.16), showing the evolution from a localised mutation at the centre. The initial conditions were the normal tissue steady state $l = 0.1, m = \upsilon, n = 0.9, f = 0, c = 0$ on the whole domain, apart from the mutation $l = 0, m = 1, n = 0, f = 0, c = 0$ for $-0.5 < x < 0.5$. The parameters are: $D_l = D_m = D_n = 5$, $D_f = 100$, $D_c = 2.5$, $\alpha = 0.01$, $\beta = 5.0$, $\delta_c = 0.5$, $\delta_f = 2.0$, $\delta_l = 0.1$, $N = 1$, $I = 0.01$, $k_1 = 10.0$, $k_2 = 0.2$, $\sigma = 58$, $\xi = 2.8$.

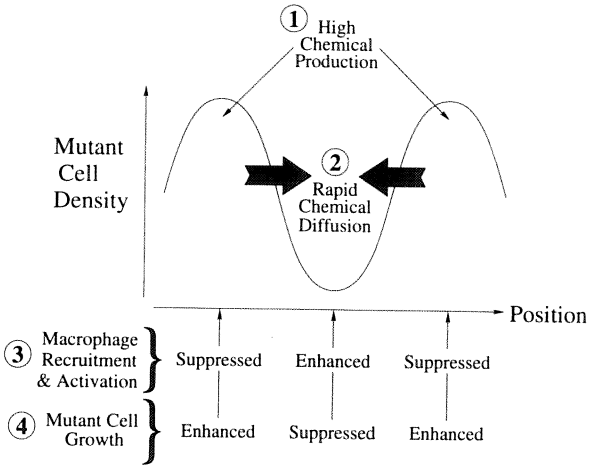

Figure 4.9 An intuitive explanation for the development of spatial inhomogeneities within a tumour, due to interactions with macrophages. A locally elevated mutant cell density is reinforced by the consequently elevated chemical regulator production (step 1) – if the chemical diffuses sufficiently fast (step 2), then local macrophage recruitment and activation will be suppressed (step 3), and hence mutant cell growth enhanced (step 4). Correspondingly, non-local recruitment and activation of macrophages will be enhanced, and mutant cell growth suppressed.

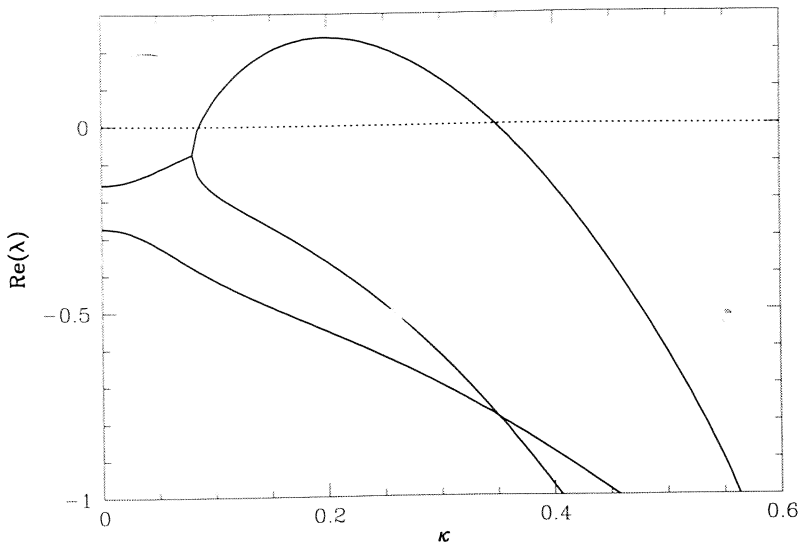

Figure 4.10 Numerically calculated dispersion relation for the model (4.16), showing $\mathrm{Re}(\lambda)$ as the wavenumber κ varies. The different curves are for different eigenvalues. For κ between about 0.09 and 0.345 the real part of one of the eigenvalues is positive, indicating that the homogeneous steady state is unstable to perturbations with those wavenumbers.

Figure 4.10 illustrates the numerically calculated dispersion relation for a parameter set for which a range of wavenumbers are unstable; Figure 4.8 shows the corresponding numerical simulation of the partial differential equations. Although the wavefront is moving, the pattern which grows behind the front is stationary in space, with a wavelength of 33 cell lengths. The wavenumber of the fastest-growing mode in the dispersion relation is approximately $\kappa = 0.2$, giving a wavelength of 31 cell lengths, in good agreement with the above observation from numerical simulations.

4.3.4 Numerical simulations in two dimensions

So far we have considered solutions in one space dimension only, but real tumours reside in a three-dimensional tissue. For any mathematical model, the range of potential solution behaviours is much greater in higher dimensions, and while numerical solution of the equations in three dimensions would be too computationally intensive for our current resources, two-dimensional simulations are feasible, and show a number of features of interest. Perhaps a central theme in the biological background to this work, and indeed in much of tumour biology, is the heterogeneity between and within tumours. It is heterogeneity within tumours that is the focus of this chapter, and we have demonstrated a possible mechanism for the development of spatial heterogeneity. The more realistic two-dimensional setting and the possibility of still greater complexity, such as an instability of the wavefront itself, is the focus of interest in an investigation of two-dimensional solutions.

The dispersion relation as calculated in Section 4.3.3, and illustrated in Figure 4.10,

is still valid, so that whenever patterns appear in one dimension they will also appear in two, but the precise nature of those patterns requires investigation. In one dimension the unstable wave number κ is a scalar, and a corresponding instability can only give rise to a single pattern, but in two dimensions the corresponding wave number (κ_x, κ_y) is two-dimensional, with $\kappa = \{\kappa_x^2 + \kappa_y^2\}^{1/2}$. If one of κ_x and κ_y is zero then the pattern will be just simple stripes, but if they are both non-zero then the pattern will be two-dimensional, tiling the plane. This introduces the possibility of more than one pattern being stable for a given parameter set, depending on the domain and initial conditions.

The model equations were solved in two dimensions using an alternating direction implicit method. This means that each time step consists of an explicit half-time step in the x direction and an implicit half-time step in the y direction, and then similar half-time steps exchanging explicit for implicit and vice versa. Figure 4.11 shows a shaded plot of the macrophage density that develops following a localised introduction of mutant cells into normal tissue. A circular travelling wave is established, behind which the tumour steady state is unstable to spatial perturbations, which leads to the formation of a stationary target pattern. The concentric rings in the circular geometry of the simulation correspond to stripes in a planar geometry; the break-up of the pattern at the centre seems likely to be due to curvature effects. Numerical simulations for the same parameters, but on a finite rectangular domain with randomly generated initial conditions, indicate that for the parameters used in the figure, both spotted and striped patterns stably coexist, with the initial conditions determining which state is reached. This is a well-known phenomenon away from a primary Turing bifurcation (Murray, 1991); note that sufficiently close to a Turing bifurcation, only one of the striped and spotted patterns can be stable (Ermentrout, 1991). However, our simulations indicate that, for the parameters in Figure 4.11, stripes always develop in the simulation of the growing tumour. In real tumours such patterns would be significantly modified by the effects of environmental noise, so the results illustrated in Figure 4.11 are not expected to represent real situations that might arise in practice. The essential implication of our results is rather that macrophage–tumour cell interactions can act as a first step in the initiation of both spatial and spatio-temporal heterogeneity.

4.3.5 Summary of model predictions

The ability of the immune system to spontaneously eliminate tumours was widely debated in the 1950s and 60s. In recent years, attention has switched to the more complex regulatory effects of the immune system on tumour progression. Our work suggests that these two philosophies are not separate, but rather have an important overlap. Our model predicts that macrophages are unable to spontaneously eliminate whole tumours, in keeping with the conventional view that, without intervention, the immune system is an ineffective weapon against the majority of cancers. Nevertheless, our model predicts that the ability of macrophages to selectively kill tumour cells has an extremely significant effect on tumour development, since it is able to induce spatial inhomogeneities. This new prediction is consistent with observations of Leek *et al.* (1996), which demonstrate the existence of macrophage hot spots within breast carcinomas, in a manner highly reminiscent of our results. Moreover, the work of Leek

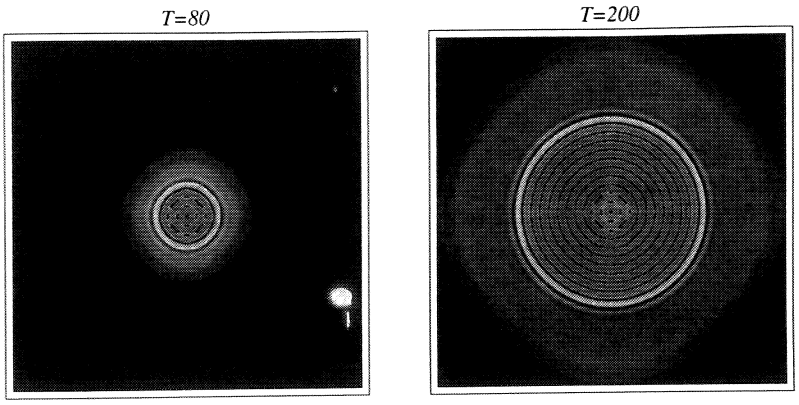

Figure 4.11 Numerical simulation in two dimensions, showing the macrophage density after 80 and 200 dimensionless time units of evolution from a single unit seeding region with a mutant cell density of 1, located at the centre of the domain. Macrophage density is represented on a grey scale, with darker colouring indicating lower cell density. The domain size is 2000×2000, and the parameters are $D_l = D_m = D_n = 5$, $D_f = 500$, $D_c = 2.5$, $\alpha = 0.01$, $\beta = 5.0$, $\delta_c = 0.5$, $\delta_f = 2.0$, $\delta_l = 0.1$, $N = 1$, $I = 0.01$, $k_1 = 10.0$, $k_2 = 0.2$, $\sigma = 40$, $\xi = 2.0$.

et al. (1996) suggests that these hot spots may play a key role in inducing tumour angiogenesis. This implies that high macrophage densities actually favour tumour progression, despite their antitumour activities, an observation made previously by Lewis *et al.*, (1995). Our work suggests that this antitumour activity may nevertheless be crucial in establishing the spatial structure that is later able to induce angiogenesis.

Experimental investigation of the predictions of our model is potentially possible using cell spheroid assays, which could in principle be seeded with macrophage cells. This line of inquiry provides the exciting possibility of providing a detailed, quantitative link between the results of a model of the type we are considering, and experimental data. This would provide a natural route towards detailed applications of our model to in vivo tumour dynamics.

REFERENCES

Adam, J.A. (1986) A simplified mathematical model of tumor growth. *Math. Biosci.*, 81: 229–244.

Adam, J.A. (1993) The dynamics of growth-factor-modified immune response to cancer growth: One dimensional models. *Mathl. Comp. Modelling*, 17: 83–106.

Adam, J.A. and Bellomo, N. (1997) *A Survey of Models for Tumor-Immune System Dynamics*. Birkhäuser.

Albert, A., Freedman, M. and Perelson, A.S. (1980) Tumors and the immune system: The effects of a tumor growth modulator. *Math. Biosci.*, 50: 25–28.

Anderson, A.R.A. and Chaplain, M.A.J. (1998) Continuous and discrete models of tumor-induced angiogenesis *Bull. Math. Biol.*, 60: 857–899.

Aznavoorian, S., Stracke, M.L., Krutzsch, H., Schiffman, E. and Liotta, L.A. (1990) Signal transduction for chemotaxis and haptotaxis by matrix molecules in tumour cells. *J. Cell Biology*, 110: 1427–1438.

Bailey, H., Love, R.J., Mann, C.V. *et al.* (1995) *Bailey and Love's Short Practice of Surgery.* Chapman and Hall.

Barr, L.C., Carter, R.L. and David, A.J.S. (1988) Encapsulation of tumors as a modified wound healing response. *The Lancet*, II: 135–137.

Berenblum, I. (1970) The nature of tumour growth. In: *General Pathology*, (Florey HEW, ed.), Lloyd-Luke.

Bottazzi, B., Polentarutti, N., Acero, R., Balsari, A., Boraschi, D., Ghezzi, P., Salmona, M. and Mantovani, A. (1983) Regulation of the macrophage content of neoplasms by chemoattractants. *Science*, 220: 210–212.

Bottazzi, B., Erba, E., Nobili, N., Fazioli, F., Rambaldi, A. and Mantovani, A. (1990) A paracrine circuit in the regulation of the proliferation of macrophages infiltrating murine sarcomas. *J. Immunol.*, 144: 2409–2412.

Burton, A.C. (1966) Rate of growth of solid tumours as a problem of diffusion. *Growth*, 30: 159–176.

Byrne, H.M. (1997) The importance of intercellular adhesion in the development of carcinomas. *IMA J. Math. Appl. Med. Biol.*, 14: 305–323.

Byrne, H.M. and Chaplain, M.A.J. (1995) Growth of nonnecrotic tumors in the presence and absence of inhibitors. *Math. Biosci.*, 130: 151–181.

Byrne, H.M. and Chaplain, M.A.J. (1996) Modelling the role of cell-cell adhesion in the growth and development of carcinoma. *Mathl. Comp. Modelling*, 24: 1–17.

Carter, R.L., Barr, L.C. and O'Brien, C.J. *et al.* (1985) Transcapsular spread of metastatic squamous cell carcinoma from cervical lymph nodes. *Am. J. Surgery*, 150: 495–499.

Chaplain, M.A.J. and Sleeman, B.D. (1990) A mathematical model for the production and secretion of tumour angiogenesis factor in tumours. *IMA J. Math. Appl. Med. Biol.*, 7: 93–108.

Chaplain, M.A.J. and Stuart, A.M. (1993) A model mechanism for the chemotactic response of endothelial cells to tumor angiogenesis factor. *IMA J. Math. Appl. Med. Biol.*, 10: 149–168.

Ermentrout, B. (1991) Stripes or spots - non-linear effects in bifurcation of reaction-diffusion equations on the square. *Proc. R. Soc. Lond. A*, 434: 413–417.

Esgro, J.J., Whitworth, P. and Fidler, I.J. (1990) Macrophages as effectors of tumor immunity. *Immunol. Allergy Clin. N. Am.*, 10: 705–729.

Fisher, R.A. (1937) The wave of advance of advantageous genes. *Ann. Eugenics*, 73: 353–369.

Folkman, J. (1995) Angiogenesis in cancer, vascular, rheumatoid and other disease. *Nature Med.*, 1: 27–31.

Greenspan, H.P. (1972) Models for the growth of a solid tumour by diffusion. *Stud. Appl. Math.*, 51: 317–340.

Groebe, K. and Mueller-Klieser, W. (1991) Distribution of oxygen, nutrient and metabolic waste concentrations in muticellular spheroids and their dependence on spheroid parameters. *Eur. J. Biophys.*, 19: 169–181.

Hamilton, T.A. and Adams, D.O. (1987) Mechanisms of macrophage-mediated tumor injury. In *Tumor Immunology - Mechanisms, Diagnosis, Therapy* (den Otter, W. and Ruitenberg, E.J. eds), pp. 89–107. Elsevier Science.

Hiernaux, J.R. and Lefever, R. (1988) Population dynamics of tumors attacked by immunocompetent killer cells. In *Theoretical Immunology*, (Perelson, A.S. ed.), volume.2, pp. 19–36. Addison Wesley.

Jonjic, N., Alberti, S., Bernasconi, S., Peri, G., Jilek, P., Anichini, A., Parmiani, G. and Mantovani, A. (1992) Heterogeneous susceptibility of human-melanoma clones to monocyte cytotoxicity – role of ICAM-1 defined by antibody blocking and gene transfer. *Eur. J. Immunol.*, 22: 2255–2260.

Kuznetsov, V.A. (1996) Harpoon model for cell-cell adhesion and recognition of target cells by the natural killer cells. *J. Theor. Biol.*, 180: 321–342.

Kuznetsov, V.A., Zhivoglyadov, V.P. and Stepanova. L.A. (1993) Kinetic approach and

estimation of the parameters of cellular interaction between the immunity system and a tumor. *Arch. Immunol. Ther. Exp.*, 41: 21–31.

Landini, G. and Rippin, J.W. (1993) Fractal dimensions of the epithelial–connective tissue interfaces in premalignant and malignant epithelial lesions of the floor of the mouth. *Anal. Quant. Cytol. Histol.* 15: 144-149.

Landini, G. and Rippin, J.W. (1996) How important is tumour shape? Quantification of the epithelial–connective tissue interface in oral lesions using local connected fractal dimension analysis. *J. Pathol.* 179: 210-217.

Leek, R.D., Lewis, C.E., Whitehouse, R., Greenall, M., Clarke, J. and Harris, A.L. (1996) Association of macrophage infiltration with angiogenesis and prognosis in invasive breast carcinoma. *Cancer Res.*, 56: 4625–4629.

Lewis, C.E., Leek, R., Harris, A.L. and McGee, J.O.D. (1995) Cytokine regulation of angiogenesis in breast cancer – the role of tumor-associated macrophages. *J. Leukoc. Biol.*, 57: 747–751.

Mace, K.F., Ehrke, M.J., Hori, K., Maccubbin, D.L. and Mihich, E. (1988) Role of tumor necrosis factor in macrophage activation and tumoricidal activity. *Cancer Res.*, 48: 5427–5432.

Mantovani, A. (1990) Tumour-associated macrophages. *Curr. Opin. Immunol.*, 2: 689–692.

Mantovani, A., Bottazzi, B., Colotta, F., Sozzani, S. and Ruco, L. (1992) The origin and function of tumor-associated macrophages. *Immunol. Today*, 13: 265–270.

Murray, J.D. (1991) *Mathematical Biology.* Springer Verlag, Berlin.

Orme, M.E. and Chaplain, M.A.J. (1996) A mathematical model of the first steps of tumour-related angiogenesis: Capillary sprout formation and secondary branching. *IMA J. Math. Appl. Med. Biol.*, 13: 73–98.

O'Sullivan, C. and Lewis, C.E. (1994) Tumor-associated leukocytes - friends or foes in breast-carcinoma. *J. Path.*, 172: 229–235.

Owen, M.R. and Sherratt, J.A. (1997) Pattern formation and spatiotemporal irregularity in a model for macrophage-tumour interactions. *J. Theor. Biol.* 189: 63–80.

Owen, M.R. and Sherratt, J.A. (1999) Mathematical modelling of macrophage dynamics in tumours. *Math. Mod. Meth. Appl. Sci.* 9: 513–539.

Owen, M.R. and Sherratt, J.A. (1998b) Modelling the macrophage invasion of tumours: effects on growth and composition. *IMA J. Math. Appl. Med. Biol.* 15: 165–185.

Parsons, D.F. (1993) Tumor cell interaction with stromal elastin and type-I collagen: The consequences of specific adhesion and proteolysis. *Tumor Biol.*, 14(3): 137–143.

Perumpanani, A.J., Sherratt, J.A., Norbury, J. and Byrne, H.M. (1996) Biological inferences from a mathematical model for malignant invasion. *Invasion and Metastasis*, 16: 209–221.

Perumpanani, A.J., Sherratt, J.A. and Norbury, J. (1997) Mathematical modelling of capsule formation and multinodularity in benign tumour growth. *Nonlinearity*, 10: 1599-1614.

Robbins, S.L., Cotran, R.S. and Kumar, V. (1984) *Pathologic Basis of Disease.* Saunders, Philadelphia; London.

Sampson-Johannes, A. and Carlino, J.A. (1988) Enhancement of human monocyte tumoricidal activity by recombinant M-CSF. *J. Immunol.*, 141: 3680–3686.

Sanchez-Garduno, F. and Maini, P.K. (1995) Travelling wave phenomena in some degenerate reaction-diffusion equations. *J. Diff. Eq.* 117: 281–319.

Sherratt, J.A. and Marchant, B.P. (1996) Non-sharp travelling waves in the Fisher equation with degenerate non-linear diffusion. *Appl. Math. Lett.*, 9: 33-38.

Sherratt, J.A. and Murray, J.D. (1991) Mathematical analysis of a basic model for epidermal wound-healing. *J. Math. Biol.*, 29: 389–404.

Sherratt, J.A. and Nowak, M.A. (1992) Oncogenes, anti-oncogenes and the immune response to cancer: A mathematical model. *Proc. R. Soc. Lond. B*, 248: 261–271.

Stetler-Stevenson, W.G., Aznavoorian, S. and Liotta, L.A. (1993) Tumor cell interactions with the extracellular matrix during invasion and metastasis. *Ann. Rev. Cell. Biol.*, 9: 541–73.

Vaidya, V.G. and Alexandro, F.J. Jr. (1982) Evaluation of some mathematical models for tumour growth. *Int. J Biomed. Comput*, 13: 19.

van Damme, J., Proost, P., Lenaerts, J.P. and Opdenakker, G. (1992) Structural and functional identification of two human, tumor-derived Monocyte Chemotactic Proteins (MCP-2 and MCP-3) belonging to the chemokine family. *J. Exp. Med.*, 176: 59–65.

Ward, J.P. and King, J.R. (1997) Mathematical modelling of avascular tumour growth. *IMA J. Math. Appl. Med. Biol.*, 14: 39–69.

Weinberg, R.A. (1989) Oncogenes, anti-oncogenes, and the molecular bases of multistep carcinogenesis. *Cancer Res.*, 49: 3713–3721.

Wheldon, T.E. (1975) Mitotic autoregulation of normal and abnormal cells: Alternative mechanisms for the derangement of growth control. *J. Theor. Biol.*, 53: 421–433.

William, P.L. and Gray, H. (1995) *Gray's Anatomy*. Churchill Livingstone.

Xie, B., Bucana, C.D., and Fidler, I.J. (1994) Density-dependent induction of 92-kd type type-IV collagenase activity in cultures of A431 human epidermoid carcinoma cells. *Am. J. Pathol.*, 144(5): 1958–67.